Received: 28 July 2020 | Revised: 30 October 2020 | Accepted: 1 November 2020

DOI: 10.1111/jace.17593

ORIGINAL ARTICLE

Journal of the American Ceramic Society

3D Nanotomography of calcium silicate hydrates by transmission electron microscopy

Panod Viseshchitra[1] | **Peter Ercius**[2] | **Paulo J. M. Monteiro**[3] | **Mary Scott**[2,4] | **Daniela Ushizima**[5,6] | **Jiaqi Li**[3] | **Ke Xu**[3] | **Hans-Rudolf Wenk**[1]

[1]Department of Earth and Planetary Science, University of California, Berkeley, CA, USA

[2]National Center for Electron Microscopy, Molecular Foundry, Lawrence Berkeley National Laboratory, Berkeley, CA, USA

[3]Department of Civil and Environmental Engineering, University of California, Berkeley, CA, USA

[4]Department of Materials Science and Engineering, University of California, Berkeley, CA, USA

[5]Computational Research Division, Lawrence Berkeley National Laboratory, Berkeley, CA, USA

[6]Berkeley Institute for Data Science, University of California Berkeley, Berkeley, CA, USA

Correspondence
Panod Viseshchitra, Department of Earth and Planetary Science, University of California, Berkeley, CA 94720, USA.
Email: panodvis@berkeley.edu

Abstract

Calcium silicate hydrate (C-S-H), is the principal hydration product of Portland cement that mainly contributes to the physical and mechanical properties of concrete. This paper aims to investigate the three-dimensional structure of C-S-H with Ca/Si ratios of 1.0 and 1.6 at the nanoscale using electron tomography. The 3D reconstructions and selected region of interest analysis confirm that the morphology of both C-S-H materials are foil-like structures. The difference between the two materials is the density of elongated structures. C-S-H with Ca/Si ratio 1.6 is clearly composed of denser particles compared to the other C-S-H material due to overlapping of the foil-like structure. Pore analysis shows that C-S-H 1.0 and C-S-H 1.6 have porosities 69.2% and 49.8% respectively. Pore size distribution also reveals that C-S-H 1.0 has pore size range between 0-250 nm and C-S-H 1.6 between 0-100 nm. The pore network's size of C-S-H 1.0 is significantly larger than 1.6. This study illustrates the capability of using electron tomography to determine the 3D nanoscale structure of cementitious products and to distinguish between C-S-H 1.0 and 1.6.

KEYWORDS

calcium silicate hydrate, morphology, portland cement, transmission electron microscopy

1 | INTRODUCTION

Portland cement-based concrete has been used as the primary construction material for the modern infrastructure during the past 65 years.[1] The reasons behind its success are attributed to the low cost and global availability of the raw materials used in Portland cement manufacture and concrete production and to its robust, excellent resistance to water, leading to a controllable and high performance behavior.[2] According to the US Geological Survey, the yearly production of Portland cement has increased dramatically in the past century, with an annual manufacture of 4.1 billion metric tons in 2018,[3] adding 2.9 billion metric tons of CO_2 into the atmosphere and contributing significantly to global warming. Green concrete contains alternative compounds to reduce the carbon footprint during manufacturing process.[4,5] It uses less energy in its production and may contain industrial by-products such as fly ash or blast furnace slag, reducing the generation of CO_2. The change in existing technologies to produce efficient green concrete requires optimization of the micro/nano structure such that less cement will be required in its manufacture. Some essential hydration products such as calcium silicate hydrate (C-S-H) consist of particles generally a few nanometers in size,[6,7] which significantly contribute to the concrete mechanical behavior.[8,9] Several imaging techniques have been used to characterize the pore network such as transmission electron microscopy (TEM),[10] focused ion beam/ scanning electron microscopy (FIB/SEM),[11,12] and X-ray imaging.[13]

The reactive Portland cement powder, mainly consisting of tricalcium silicate (Ca_3SiO_5, or C_3S in the cement notation) and dicalcium silicate (Ca_2SiO_4, or C_2S), can be mixed with water to produce a hardened material through complex reactions that produce the main binding product: calcium silicate hydrate (C-S-H).

C-S-H formed during the hydration process is the key binding phase and primary contributor to the mechanical properties of most hydrated Portland cement and concretes. The C-S-H phases have poorly ordered crystal structures resembling the mineral tobermorite ($Ca_5Si_6O_{16}(OH)_2{\cdot}7H_2O$).[14,15] The crystal structure of 14 Å tobermorite consists of complex layers of central octahedral calcium oxide sheets with tetrahedral silicate chains on both sides, which are attached with a periodicity of three tetrahedra (Figure 1). The space between two complex layers contains additional calcium cations and H_2O. The poor crystallinity and short-range order character of C-S-H have prevented a satisfactory structural description with X-ray diffraction techniques.[16] To better understand the C-S-H structure, a precise three-dimensional model of C-S-H at the nanoscale is needed.

The porosity of C-S-H plays a key role in the durability-based performance of concrete. The size distribution and connectivity of the pores determine the ability of fluids and ions to flow through the network, potentially degrading the material. Both the porosity and the pore size distribution are determined by the nanostructure of C-S-H. To date, there have been several studies on the nanostructure and morphology of a variety of Portland-cement-based systems.[17-21] While such studies answer many questions, such as phase development in the system, the results of these techniques, including scanning electron microscopy are distilled into two-dimensional (2D) information that provide only limited, often inferred, volumetric information of the nanostructure, and the pore network for a bulk paste. Simulations can also be used for these investigations.[22,23] Due to the complex nature of cement hydration and the sensitivity of the products formed, only a few studies of the three-dimensional (3D) structure at the nanoscale have been completed.[24]

Transmission electron microscopy (TEM) can image specimens at very high resolution. It is widely used in materials science including observations of cement, for example, to observe the morphology of hydration products of cements.[17,25-28] to characterize the effect of mineral admixtures, such as metakaolin,[29] on the hydration reactions.[30] Electron tomography uses TEM images to reconstruct the 3D structure of an object from a series of projection images from different viewing angles. This method has been applied to many porous systems in materials science such as in imaging of nanoscale dendrites.[31] A recent study[10] used electron tomography to investigate the nanostructure and pore network of C-S-H and found two separate networks of pores that are most likely attributed to two particles of the same phase in different orientations. Due to sensitivity of C-S-H to the electron beam, beam damage still occurred and improvements are needed to develop a robust protocol for TEM tomographic studies of cementitious materials. To acquire a tomographic tilt series, the sample is rotated and a series of 2D projection images is measured at different tilt angles.[32] This research studied synthetic C-S-H instead of hydrated C3S because of the desire to have only one phase in the system. The 3D reconstruction method used in this experiment is the simultaneous iterative reconstruction technique (SIRT) method.[33] This study aims to investigate and compare the 3D structure of C-S-H with Ca/Si ratios of 1.0 and 1.6 at the nanoscale using 3D electron tomography. The resulting information of pore analysis is critical for the development of a new generation of optimized green cement.

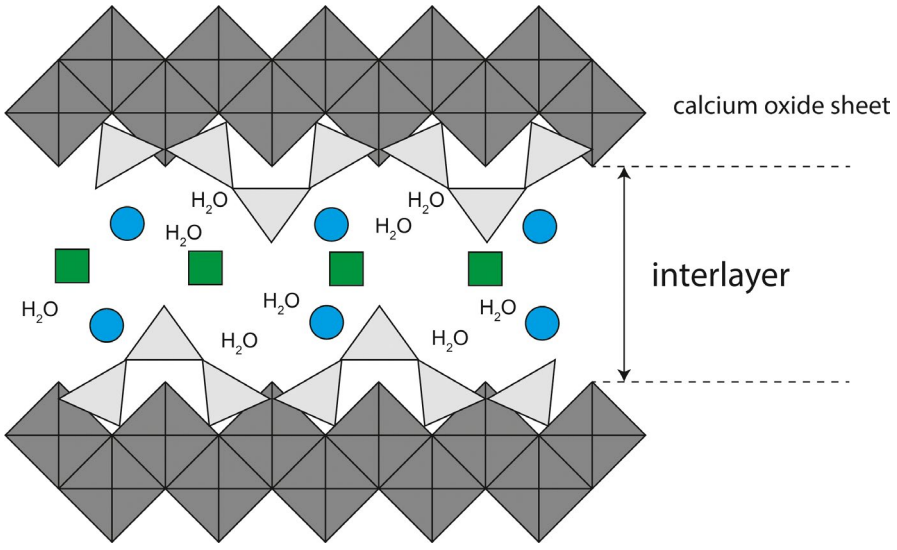

FIGURE 1 Schematic of the atomic structure of C-S-H. The layers of octahedral calcium oxide sheet are drawn in dark grey, whereas the light grey triangles are SiO_4^{4-} tetrahedra. The interlayer contains water and positively-charged species (blue circles and green squares, respectively) that can neutralize the structure (eg Ca^{2+} and/or K^+)[15] [Color figure can be viewed at wileyonlinelibrary.com]

2 | EXPERIMENTAL METHODS

2.1 | Materials

The samples in this work is the same materials to this publication.[34] C-S-H was synthesized by mixing calcium oxide (CaO) and silica fume (SiO_2) at Ca/Si molar ratios 1.0 (C-S-H 1.0) and 1.6 (C-S-H 1.6) with water. The water to solid ratio of both samples is equal to 45. CaO was obtained by burning calcium carbonate ($CaCO_3$, Merck, pro analysis) at 1000°C for 12 hours. SiO_2, provided by Aerosil 200, Evonik, was chosen for its high specific surface area. The synthesis process and all the sample handling were carried out in a N_2 filled glovebox to prevent CO_2 contamination. The samples were stored in 100 mL high-density polyethylene (HDPE) containers placed on a shaker moving at 100 rpm and equilibrated at 20°C. For each equilibration time, a separate sample was prepared. After equilibrated for 182 days, the solid and the liquid phase were separated by filtration using a 0.45 μm nylon filter. The solid phase for both Ca/Si ratio was analyzed by X-ray diffractometry (XRD) and only C-S-H is observed. There is no portlandite nor evidence of carbonation. The XRD results are shown in Figure 2.

2.2 | Electron tomography

The electron tomography requires several steps including sample preparation, data acquisition, data alignment, data reconstruction, and object visualization. The C-S-H sample was suspended in ethanol and deposited on a 200 mesh ultra-thin copper hexagonal grid with carbon film support (CF200H-Cu-UL, Electron Microscopy Sciences). 10 nm gold fiducial markers (Aldrich) were deposited to aid in tilt series alignment. Data acquisition was acquired on a Tecnai 12 TEM, operating at 120 kV. The C-S-H 1.0 was rotated around one axis from −40° to +70° with 1° angle increment producing 111 projection images. The C-S-H 1.6 was rotated around one axis from −60° to +60° with 1.56° angle increment, producing 76 projection images. All images were acquired automatically using the SerialEM software.

The alignment, reconstruction were done using the IMOD software.[35] Visualization of the reconstructed volume was done either by volume or surface rendering. The volume rendering was optimized by manually adjusting the color and the transparency. The visualizations were done using the Tomviz 1.8 software.[36] IMOD and Tomviz are open source software for volumetric data processing and visualization, especially for electron tomography.

2.3 | Model analysis

The geometrical information of all particles (ROIs) was obtained from the Tomviz software. The selected ROIs are cropped and object sizes were measured using the ruler function. The pore analysis of the reconstructed models was obtained using the Fiji/ImageJ software. The segmentation, which allows to isolate pores with respect to C-S-H, is based on global thresholding with the Otsu algorithm.[37] The porosity is calculated based on the ratio of the white area (particles) divided by the total area. The continuous pore size distribution (CPSD) and continuous pore size distribution with mercury intrusion porosimetry simulation (CMIP) were determined using the Xlib plugin[12] in ImageJ. For CPSD, the pore space is separated into regions of different radii that can be filled with objects of different radii.[12] The sizes of these radii are attached to the respective locations. For CMIP, same PSD definition as for the CPSD. However, the balls of different radii are intruded into the pore volume from one of the faces of the 3D image cube or from one of the edges of the 2D image, respectively. This definition of the PSD corresponds to the data that are collected by mercury intrusion porosimetry (MIP).[12]

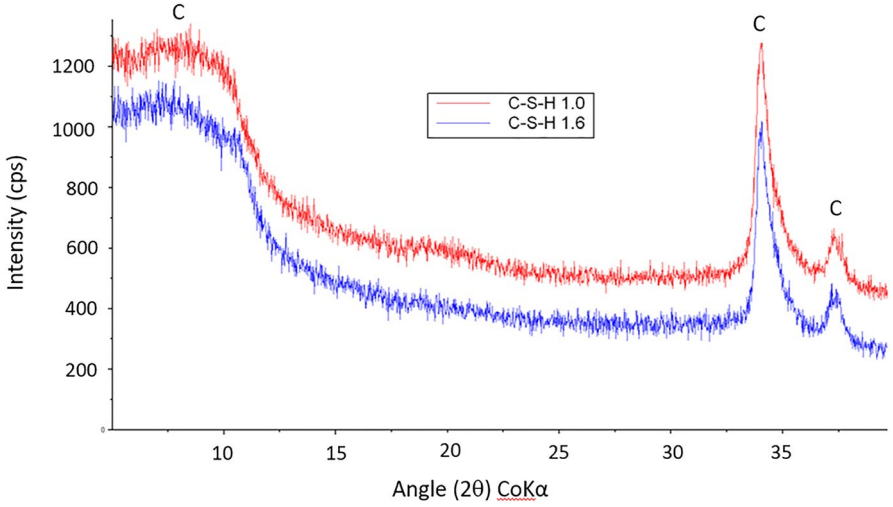

FIGURE 2 XRD results of C-S-H 1.0 (red line) and C-S-H 1.6 (blue line). Three main peaks of C-S-H are at around 8°, 34°, and 37° 2θ [Color figure can be viewed at wileyonlinelibrary.com]

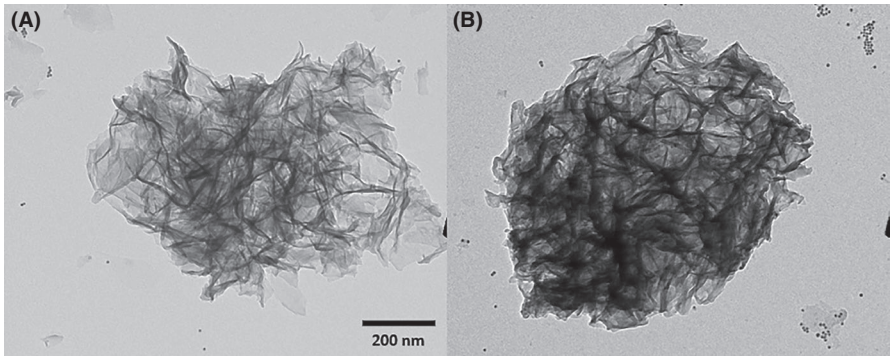

FIGURE 3 Two 2D images of C-S-H with Ca/Si ratio 1.0 (A) and ratio 1.6 (B) at 0° rotation

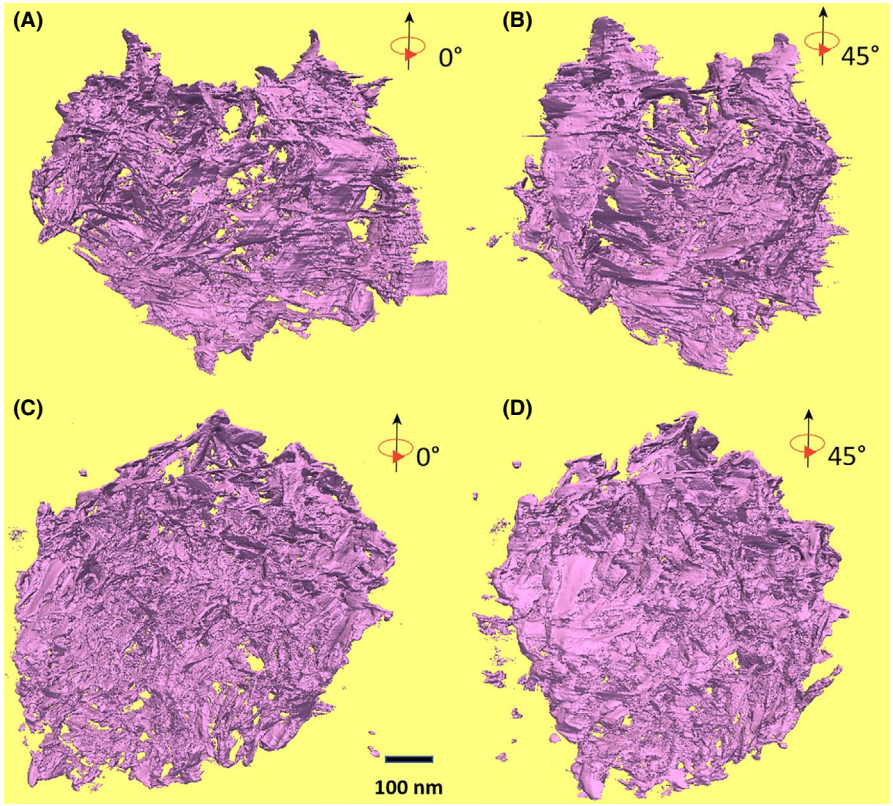

FIGURE 4 The 3D reconstruction of C-S-H 1.0 (A-B) 1.6 (C-D) at 0° and 45° rotation [Color figure can be viewed at wileyonlinelibrary.com]

3 | RESULTS

Beam damage is a major problem in electron tomography. Our particles were sensitive to beam irradiation so we were careful to limit the dose and to check for damage before 3D reconstruction. A beam dose of 5000 $e^-/(nm^2\ s)$ is suitable for this research. The example of effect of beam damage are shown in Appendix A.

Brightfield TEM images of two C-S-H particles of each ratio are given in Figure 3. We can see that the C-S-H morphology in the system is a combination of foil-like structures and elongated (fiber-like) structure. The C-S-H 1.6 appears to have a denser structure than C-S-H 1.0. However, these particles have a complex 3D morphology and simple 2D TEM projection images are insufficient to describe the morphology.

The morphologies of C-S-H are determined by the structure and chemical composition and/or kinetically of the hydration reaction.[38] Figure 4 shows isosurface renderings of the reconstructed 3D structure of C-S-H 1.0 and 1.6. The voxel size of both models is 1.14 nm. The morphologies of both C-S-H are made up of elongated, connected structures with different orientations. The C-S-H 1.6 also shows a higher density of these structures compared to C-S-H 1.0.

Next, we will take a closer look at the elongated regions of interest (ROIs) to investigate the underlying morphology at higher resolution. Elongated ROIs refer to foil-like structures that are perceived as fibers when observing the original 2D projection images of such structures. Five ROIs were selected for each sample (Figure 5). The particles sit randomly on a TEM grid. The original projection direction with the grid approximately flat (Figures 3 and

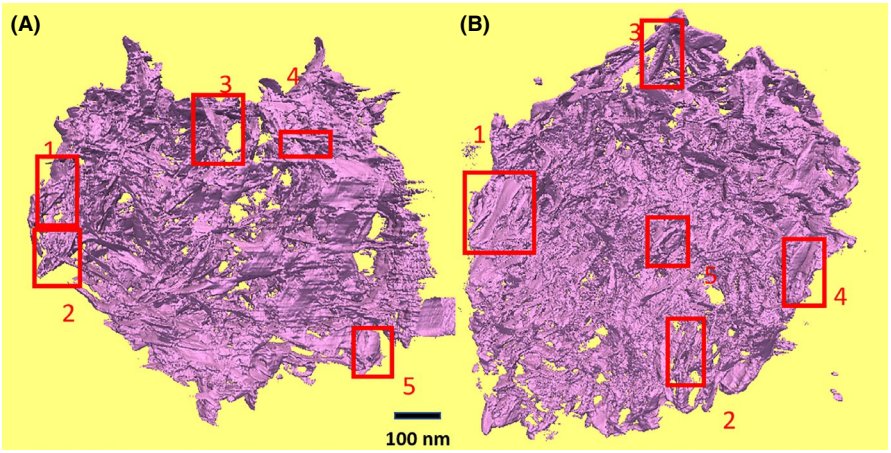

FIGURE 5 Five selected elongated ROIs of C-S-H 1.0 (A) and 1.6 (B) indicated by red rectangles [Color figure can be viewed at wileyonlinelibrary.com]

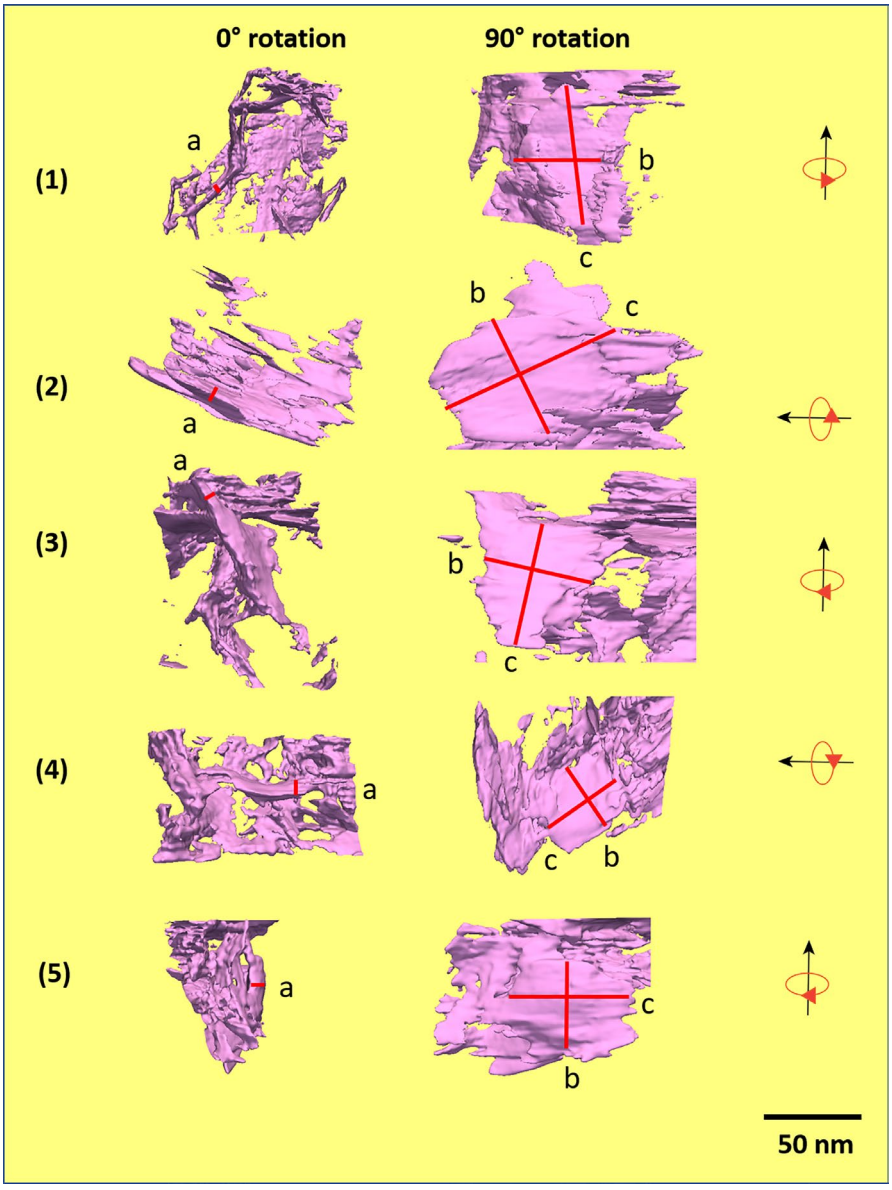

FIGURE 6 Morphologies of five selected elongated ROIs of C-S-H 1.0 [Color figure can be viewed at wileyonlinelibrary.com]

4) is arbitrary set as 0-degree rotation. Then we rotate 90° around the parent fiber direction. Each ROI is shown in 0° rotation and 90° rotation (Figure 6 for C-S-H 1.0 and Figure 7 for C-S-H 1.6). The actual geometry and aspect ratios of these ROIs are shown in Table 1. The thickness (a) of each ROI can be determined from the orientation

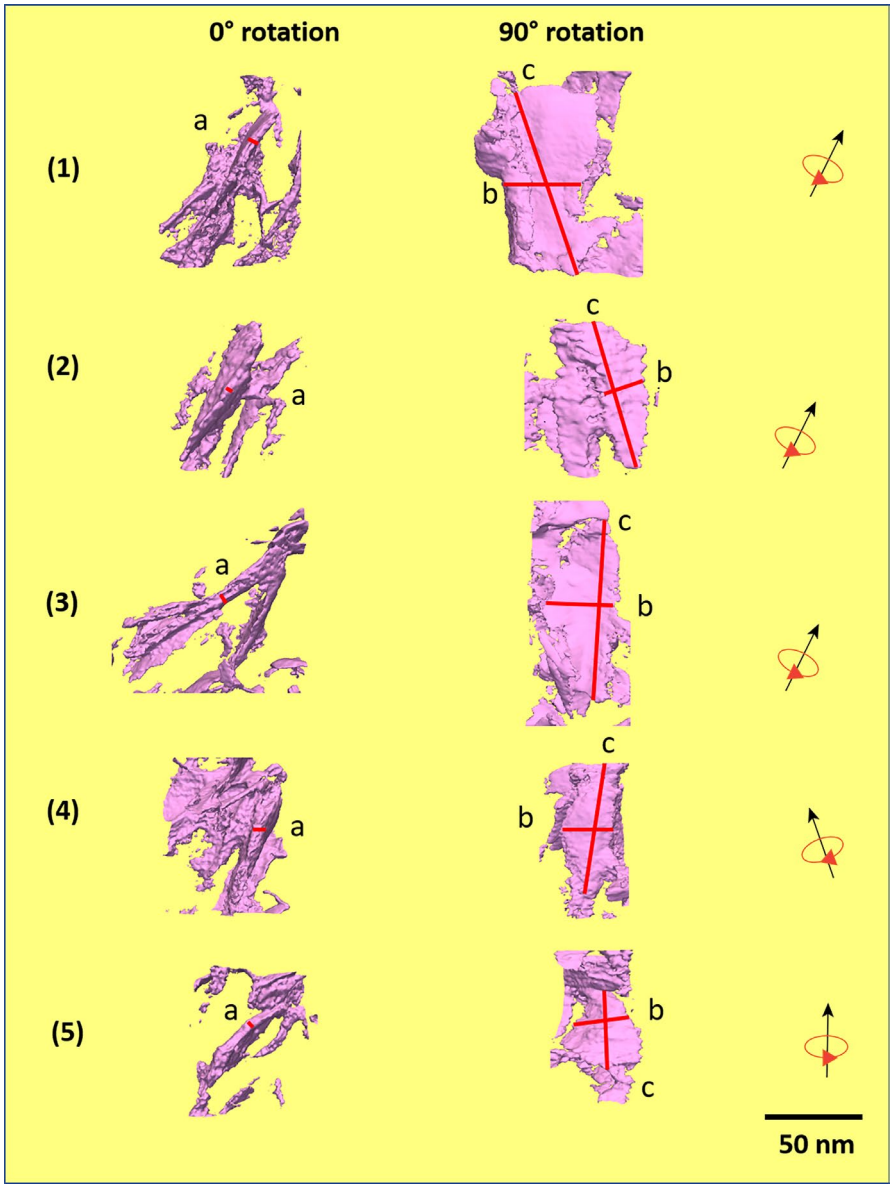

FIGURE 7 Morphologies of five selected elongated ROIs of C-S-H 1.6 [Color figure can be viewed at wileyonlinelibrary.com]

looking along the plate. The width (b) and length (c) can be determined from the direction normal to the plate. The thickness (a), width (b) and length (c) are represented by red lines in both Figures 6 and 7. Both 2D aspect ratios have high values (more than 5) indicating that all of them are elongated platelets, not fibers.

The pore analysis shows that C-S-H 1.0 and C-S-H 1.6 have porosities 69.2% and 49.8% respectively. Continuous pore size distribution (CPSD) and Continuous pore size distribution with MIP simulation (CMIP) was analyzed in this research (Figure 8). Both CPSD and CMIP reveal that C-S-H 1.0 has pore size range between 0-250 nm and C-S-H 1.6 between 0 and 100 nm. For CPSD (Figure 8A), the average pore size of C-S-H 1.0 and 1.6 are 72.0 nm and 26.4 nm respectively. However, C-S-H 1.6 has a high number of small pore volume less than 50 nm. For CMIP (Figure 8C), The average pore size of C-S-H 1.0 and 1.6 are 57.1 nm and 16.0 nm, respectively. C-S-H 1.0 has three dominant peaks at 24.2, 28.6, and 41.8 nm. while C-S-H 1.6 has only one dominant peak at 13.2 nm.

4 | DISCUSSION

From overviews of 2D images and 3D reconstructions, both samples have morphologies of elongated and foil-like structures. However, only when the selected elongated structures were tilted, they clearly display that the elongated structures are also foil-like structures and not fibers. The real C-S-H morphologies for both Ca/Si ratio 1.0 and ratio 1.6 in the system are all foil-like structures, with no evidence for fibrous structures in both the samples. The C-S-H 1.6 sample had denser particles than C-S-H 1.0. The denser structures of C-S-H 1.0 come from the overlapping of the foil-like structure. However, the morphologies of C-S-H that came from

TABLE 1 Actual geometry and aspect ratio of selected ROIs of both samples

Sample	Thickness (a) (nm)	Width (b) (nm)	Length (c) (nm)	2D Aspect ratio (b/a)	2D Aspect ratio (c/a)
C-S-H 1.0					
Particle 1	7.15	73.00	149.00	10	21
Particle 2	7.76	84.89	171.52	11	22
Particle 3	6.06	76.89	106.24	13	18
Particle 4	6.32	68.11	78.97	11	12
Particle 5	5.46	62.10	99.37	11	18
C-S-H 1.6					
Particle 1	8.13	58.85	141.06	7	17
Particle 2	4.27	56.05	83.16	13	19
Particle 3	10.19	49.82	156.05	5	15
Particle 4	4.94	42.50	94.80	9	19
Particle 5	3.83	37.63	76.40	10	20

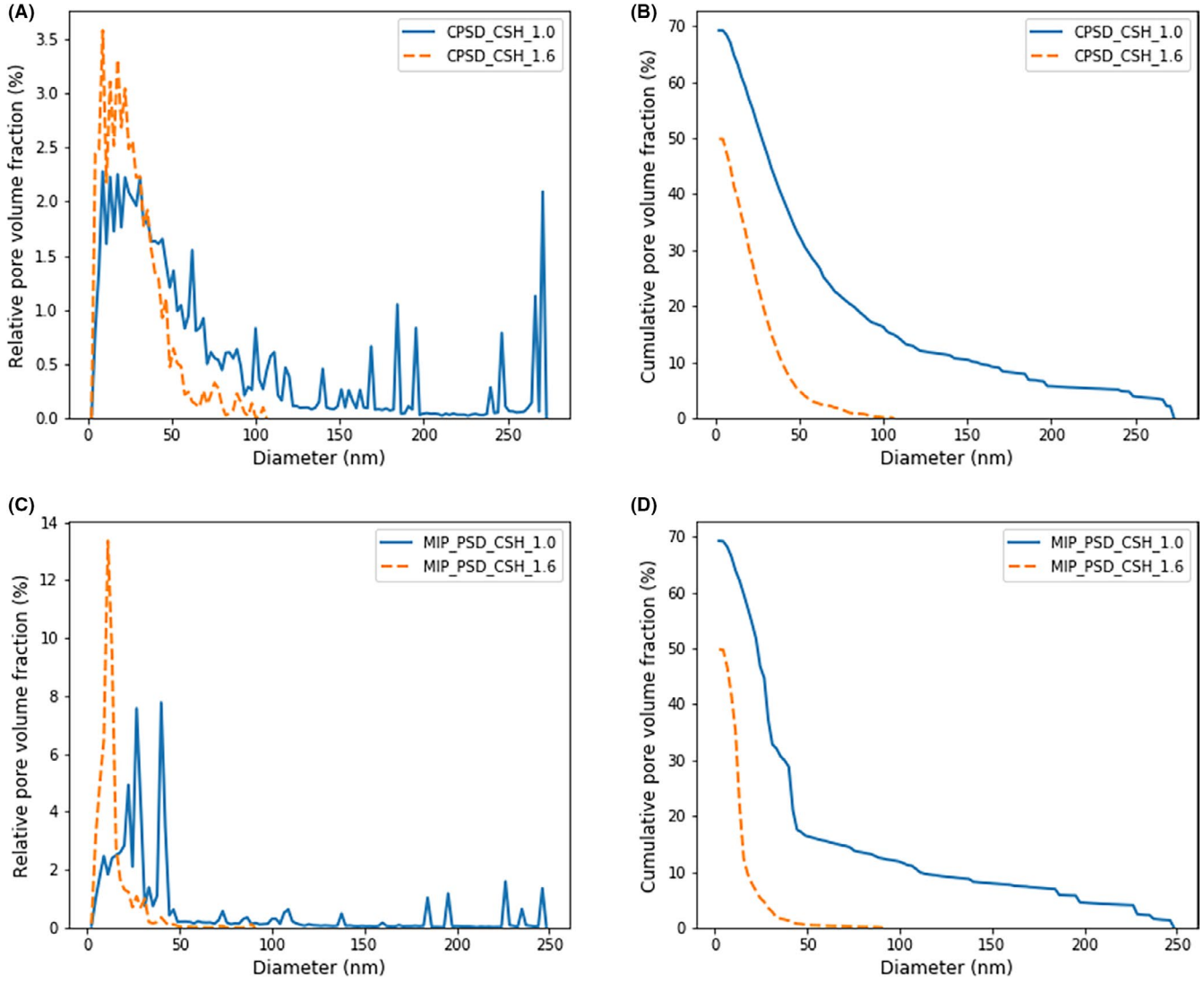

FIGURE 8 Pore size distributions of both samples: (A) Continuous pore size distribution (CPSD), (B) Cumulative continuous pore size distribution (CCPSD), (C) Continuous pore size distribution with MIP simulation (CMIP), (D) Cumulative continuous pore size distribution with MIP simulation (CCMIP) [Color figure can be viewed at wileyonlinelibrary.com]

cement paste or hydrated C_3S depend on the lime concentration. Low lime concentrations (Ca/Si ratio < 1.4) during synthesized will yield foil-like structures. High lime concentration (Ca/Si ratio > 1.6) will yield fibrous structures.[39]

The pore analysis in ImageJ, which was based on segmentation by Otsu algorithm, reveals that C-S-H 1.0 has higher porosity than C-S-H 1.6. The cumulative pore size distribution for both CPSD and CMIP (Figure 7B,D) also indicate that C-S-H 1.0 has higher porosity than C-S-H 1.6. The peak pore size for C-S-H 1.6 (Figure 7A,C) ranges from 0 to 50 nm while for C-S-H 1.0 it ranges from 0 to 250 nm. There are also peaks with pore size larger than 100 nm for C-S-H 1.0 (Figure 7A,C) which means, the pore network's size of C-S-H 1.0 is significantly larger than of C-S-H 1.6.

TEM tomography is a powerful technique to illustrate the 3D reconstruction of microstructures. However, there are some limitations. First, fiducial markers are required. To align the data set, high-contrast reference points are needed. In this experiment 10 nm gold particles were used as a fiducial marker. Second, we can reach the magnification 18,500× with equal to the beam dose of is 5000 $e^-/(nm^2\ s)$ for both C-S-H 1.0 and 1.6. For these magnifications, it is difficult to analyze the very small intralayer pore structure. To go to higher magnification, Cryo-TEM is suggested because it can reduce the beam damage. Scanning transmission electron microscope (STEM) is another method that may work. STEM satisfies the incoherent imaging approximation in which diffraction and phase contrast is decreased, and the image intensity depends on the sample thickness and the atomic number.[40] Also, the digital control of the beam in STEMs can minimize radiation damage.[41]

For the 3D nanostructure analysis based on TEM images, These two samples are synthetic samples because of the desire to have only one phase in the system so if the sample of Portland cement is analyzed, the image reconstruction and segmentation will be harder to do accurately because there are many phases in the system. In previous publications,[42,43] the authors proposed an automated image processing pipeline with machine learning-based classifiers, which achieved accurate multiphase segmentation results for the 3D X-ray micro-tomography images of ancient Roman concrete samples. Similar methods can be used for the image segmentation of TEM tomography of real samples of Portland cement in the future study.

5 | CONCLUSION

This study uses TEM tomography with simultaneous iterative reconstruction technique (SIRT) to generate the 3D reconstruction of C-S-H 1.0 and 1.6 microstructures which can be found in Portland cement paste or C_3S paste. The projection images were aligned using the 10 nm gold nanoparticles as references. The highest beam dose that can achieve this with a little beam damage is 5000 $e^-/(nm^2\ s)$ for both Ca/Si ratio 1.0 and 1.6. To obtain higher magnification and improve the quality of the reconstruction, Cryo-TEM or STEM may provide better results. The 3D reconstructions and selected ROI analysis confirm that the morphology of both C-S-H 1.0, and 1.6 are foil-like structures. The difference between two Ca/Si ratios is the density of particles. The C-S-H 1.6 shows clearly more densely packed structures compared to C-S-H 1.0 due to the overlapping of the foil-like structure. The pore analysis shows that C-S-H 1.6 has lower porosity than C-S-H 1.0. The CPSD and CMIP reveal that C-S-H 1.0 has pore size between 0-250 nm and C-S-H 1.6 between 0-100 nm and C-S-H 1.0 has pore network's size larger than C-S-H 1.6. TEM tomography shows the capability to determine the 3D nanostructure and pore networks of C-S-H and in the future related cementitious materials such as calcium alumino silicate hydrate (C-A-S-H) should be investigated.

ACKNOWLEDGMENTS

This publication is based on studies that are financially supported by SCG Cement-Building Material Co., Ltd, Bangkok, Thailand. We thank the staff at the University of California Berkeley Electron Microscope Laboratory for advice and assistance in electron microscopy sample preparation and data collection. The authors also thank Rohan Dhall from National Center for Electron Microscopy (NCEM) for the assistance of sample preparation. The work performed at the Molecular Foundry, Lawrence Berkeley National Laboratory was supported by the US Department of Energy under contract no. DE-AC02-05CH11231. HRW acknowledges support from NSF (EAR 1343908, CSEDI-106751) and DOE (DE-FG02-05ER15637).

ORCID

Panod Viseshchitra https://orcid.org/0000-0001-5364-3876
Peter Ercius https://orcid.org/0000-0002-6762-9976
Paulo J. M. Monteiro https://orcid.org/0000-0002-6866-1783
Daniela Ushizima https://orcid.org/0000-0002-7363-9468
Jiaqi Li https://orcid.org/0000-0003-4863-6641
Hans-Rudolf Wenk https://orcid.org/0000-0001-6641-7640

REFERENCES

1. Monteiro PJM, Miller SA, Horvath A. Towards sustainable concrete. Nat Mater. 2017;16(7):698–9.
2. Mehta PK, Monteiro PJ. Concrete Microstructure, Properties, and Materials, 5th edn. New York: McGraw-Hill Companies; 2014.
3. U.S. Geological Survey. Cement Statistics and Information [Internet]. 2018. Available from: https://minerals.usgs.gov/minerals/pubs/commodity/cement/
4. Phair JW. Green chemistry for sustainable cement production and use. Green Chem. 2006;8(9):763–80.
5. Imbabi MS, Carrigan C, McKenna S. Trends and developments in green cement and concrete technology. Int J Sustain Built Environ. 2012;1(2):194–216.

6. McDonald PJ, Rodin V, Valori A. Characterisation of intra- and inter-C–S–H gel pore water in white cement based on an analysis of NMR signal amplitudes as a function of water content. Cem Concr Res. 2010;40(12):1656–63.
7. Scrivener KL, Nonat A. Hydration of cementitious materials, present and future. Cem Concr Res. 2011;41(7):651–65.
8. Scrivener KL, Crumbie AK, Laugesen P. The interfacial transition zone (ITZ) between cement paste and aggregate in concrete. Interface Sci. 2004;12(4):411–21.
9. Königsberger M, Hlobil M, Delsaute B, Staquet S, Hellmich C, Pichler B. Hydrate failure in ITZ governs concrete strength: a micro-to-macro validated engineering mechanics model. Cem Concr Res. 2018;103:77–94.
10. Taylor R, Sakdinawat A, Chae SR, Wenk H-R, Levitz P, Sougrat R, et al. Developments in TEM nanotomography of calcium silicate hydrate. Jennings H, editor. J Am Ceram Soc. 2015;98(7):2307–12.
11. Holzer L, Gasser P, Muench B. Quantification of capillary pores and hadley grains in cement paste using FIB-nanotomography. Measuring, Monitoring and Modeling Concrete Properties. In: Konsta-Gdoutos MS, editor. Dordrecht: Springer Netherlands; 2006. p. 509–516.
12. Münch B, Holzer L. Contradicting geometrical concepts in pore size analysis attained with electron microscopy and mercury intrusion. J Am Ceram Soc. 2008;91(12):4059–67.
13. Bossa N, Chaurand P, Vicente J, Borschneck D, Levard C, Aguerre-Chariol O, et al. Micro- and nano-X-ray computed-tomography: a step forward in the characterization of the pore network of a leached cement paste. Cem Concr Res. 2015;67:138–47.
14. Taylor HFW. Cement Chemistry, 2nd edn. London: Thomas Telford; 1997.
15. Bonaccorsi E, Merlino S, Kampf AR. The crystal structure of tobermorite 14 Å (plombierite), a C-S–H phase. J Am Ceram Soc. 2005;88(3):505–12.
16. Taylor H. F. W. Tobermorite, jennite, and cement gel. Zeitschrift für Kristallographie - Crystalline Materials. 1992;202: 1-4:http://dx.doi.org/10.1524/zkri.1992.202.14.41.
17. Taylor R, Richardson IG, Brydson RMD. Composition and microstructure of 20-year-old ordinary Portland cement–ground granulated blast-furnace slag blends containing 0 to 100% slag. Cem Concr Res. 2010;40(7):971–83.
18. Korpa A, Kowald T, Trettin R. Phase development in normal and ultra high performance cementitious systems by quantitative X-ray analysis and thermoanalytical methods. Cem Concr Res. 2009;39(2):69–76.
19. Richardson IG. Nature of the hydration products in hardened cement pastes. Cem Concr Compos. 2000;22(2):97–113.
20. Bae S, Taylor R, Hernández-Cruz D, Yoon S, Kilcoyne D, Monteiro PJM. Soft x-ray spectromicroscopic investigation of synthetic C-S-H and C3S hydration products. J Am Ceram Soc. 2015;98(9):2914–20.
21. Bae S, Taylor R, Shapiro D, Denes P, Joseph J, Celestre R, et al. Soft X-ray ptychographic imaging and morphological quantification of calcium silicate hydrates (C–S–H). J Am Ceram Soc. 2015;98(12):4090–5.
22. Navi P, Pignat C. Three-dimensional characterization of the pore structure of a simulated cement paste. Cem Concr Res. 1999;29(4):507–14.
23. Garboczi EJ, Bentz DP. Computer simulation of the diffusivity of cement-based materials. J Mater Sci. 1992;27(8):2083–92.
24. Song Y, Davy CA, Troadec D, Bourbon X. Pore network of cement hydrates in a High Performance Concrete by 3D FIB/SEM — Implications for macroscopic fluid transport. Cem Concr Res. 2019;115:308–26.
25. Richardson IG, Skibsted J, Black L, Kirkpatrick RJ. Characterisation of cement hydrate phases by TEM, NMR and Raman spectroscopy. Adv Cem Res. 2010;22(4):233–48.
26. Richardson IG. The nature of C-S-H in hardened cements. Cem Concr Res. 1999;29(8):1131–47.
27. Richardson IG. The calcium silicate hydrates. Cem Concr Res. 2008;38(2):137–58.
28. Richardson IG, Groves GW. Models for the composition and structure of calcium silicate hydrate (C-S-H) gel in hardened tricalcium silicate pastes. Cem Concr Res. 1992;22(6):1001–10.
29. Trusilewicz L, Fernández-Martínez F, Rahhal V, Talero R. TEM and SAED characterization of metakaolin. pozzolanic activity. J Am Ceram Soc. 2012;95(9):2989–96.
30. Bullard JW, Jennings HM, Livingston RA, Nonat A, Scherer GW, Schweitzer JS, et al. Mechanisms of cement hydration. Cem Concr Res. 2011;41(12):1208–23.
31. Saghi Z, Xu X, Möbus G. Three-dimensional metrology and fractal analysis of dendritic nanostructures. Phys Rev B. 2008;78(20):205428.
32. Ercius P, Alaidi O, Rames MJ, Ren G. Electron tomography: a three-dimensional analytic tool for hard and soft materials research. Adv Mater. 2015;27(38):5638–63.
33. Miao J, Ercius P, Billinge SJL. Atomic electron tomography: 3D structures without crystals. Science (80-). 2016;353(6306):aaf2157.
34. L'Hôpital E, Lothenbach B, Kulik DA, Scrivener K. Influence of calcium to silica ratio on aluminium uptake in calcium silicate hydrate. Cem Concr Res. 2016;1(85):111–21.
35. Kremer JR, Mastronarde DN, McIntosh JR. Computer visualization of three-dimensional image data using IMOD. J Struct Biol. 1996;116(1):71–6.
36. Levin BDA, Jiang Y, Padgett E, Waldon S, Quammen C, Harris C, et al. Tutorial on the visualization of volumetric data using tomviz. Micros Today. 2018;26(1):12–7.
37. Otsu N. A threshold selection method from gray-level histograms. IEEE Trans Syst Man Cybern. 1979;9(1):62–6.
38. Richardson IG. Tobermorite/jennite- and tobermorite/calcium hydroxide-based models for the structure of C-S-H: applicability to hardened pastes of tricalcium silicate, β-dicalcium silicate, Portland cement, and blends of Portland cement with blast-furnace slag, metakaol. Cem Concr Res. 2004;34(9):1733–77.
39. Tajuelo Rodriguez E, Richardson IG, Black L, Boehm-Courjault E, Nonat A, Skibsted J. Composition, silicate anion structure and morphology of calcium silicate hydrates (C-S-H) synthesised by silica-lime reaction and by controlled hydration of tricalcium silicate (C3S). Adv Appl Ceram. 2015;114(7):362–71.
40. LeBeau JM, Findlay SD, Allen LJ, Stemmer S. Quantitative atomic resolution scanning transmission electron microscopy. Phys Rev Lett. 2008;100(20):206101.
41. Marks LD. Experimental studies of small particle structures. Rep Progr Phys. 1994;57(6):603–49

42. Ushizima D, Xu K, Monteiro PJM. Materials data science for microstructural characterization of archaeological concrete. MRS Adv. 2020;5(7):305–18.
43. Xu K, Tremsin AS, Li J, Ushizima DM, Davy CA, Bouterf A, et al. Microstructure and water absorption of ancient concrete from Pompeii: An integrated synchrotron microtomography and neutron radiography characterization. Cem Concr Res. 2021;139:106282.

How to cite this article: Viseshchitra P, Ercius P, Monteiro PJM, et al. 3D Nanotomography of calcium silicate hydrates by transmission electron microscopy. *J Am Ceram Soc*. 2021;104:1852–1862. https://doi.org/10.1111/jace.17593

APPENDIX A

Example of beam damage

Figure 9B shows the serious beam damage. The whole particle is almost destroyed. Figure 9D shows almost no beam damage. The particle is almost the same.

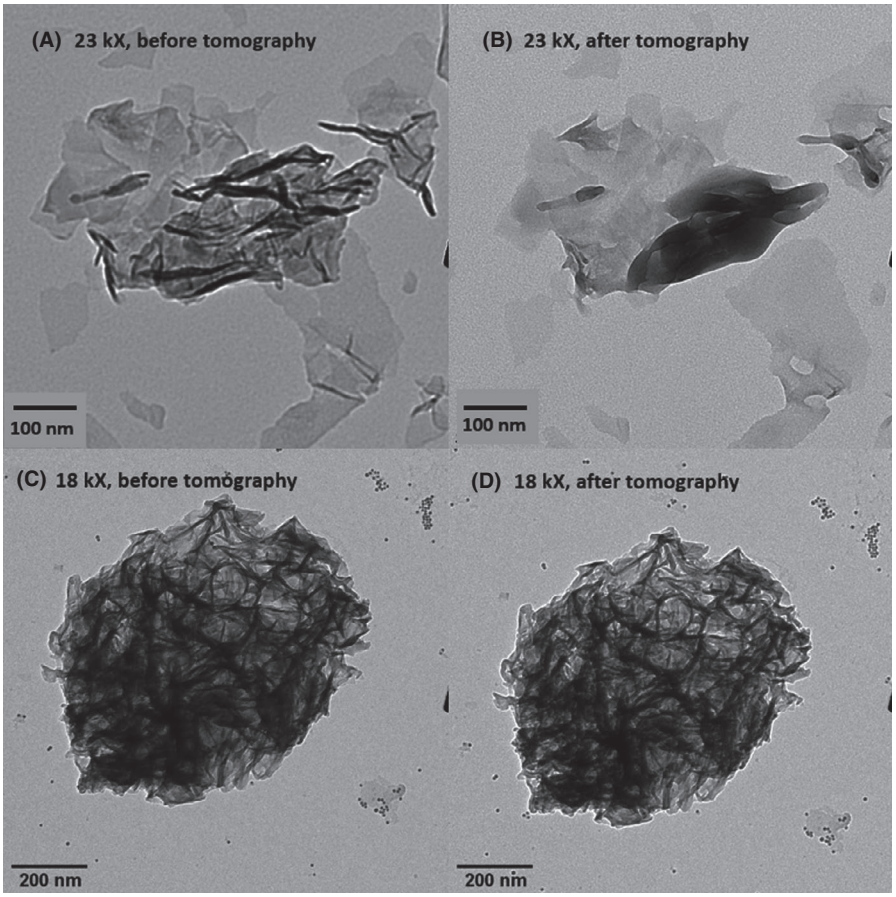

FIGURE 9 Compare the 2D images of C-S-H 1.6 at 0° rotation (A) before and (B) after tomography at 23 kX magnification. (C) before and (D) after tomography at 18 kX magnification

APPENDIX B

Example of image segmentation from otsu algorithm

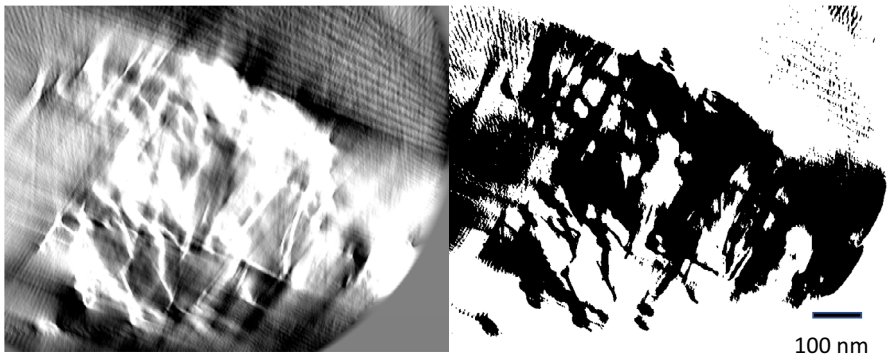

FIGURE 10 Example of segmentation of a greyscale image (left) of C-S-H 1.0 with otsu algorithms (right). The segmented black phase in the segmented image is C-S-H (solid phase) and the segmented white phase is pore phase [Color figure can be viewed at wileyonlinelibrary.com]